Selective autophagic degradation of glycolytic activator PFKFB3 contributes to maintaining intestinal epithelial barrier in inflammatory bowel disease

YIYANG PAN[1*], FENG YANG[1*], LIUCAN WANG[2*], TIANSHU YANG[1], GUANGSHENG DU[1], CONG XU[1], HUA YANG[2], MIN YU[2] and WEIDONG XIAO[1]

[1]General Surgery Laboratory, Department of General Surgery, Xinqiao Hospital, Army Medical University, Chongqing 400037, P.R. China; [2]General Surgery Laboratory, Department of General Surgery, Chongqing General Hospital, Chongqing University, Chongqing 401147, P.R. China

Received April 21, 2025; Accepted October 31, 2025

DOI: 10.3892/ijmm.2025.5714

Abstract. Inflammatory bowel disease (IBD) is a chronic idiopathic intestinal inflammatory disease with increasing incidence worldwide. However, the treatment of IBD is still limited and has not reached the expected therapeutic effect and new therapeutic targets are still to be discovered. Impaired autophagy and abnormal glycolysis levels were observed both in the *in vivo* and *in vitro* intestinal inflammation models, suggesting a relationship between autophagy and glycolysis in IBD. Subsequently, it demonstrated that autophagy negatively regulated the glycolysis of IECs by degradation of the key glycolytic enzyme 6-phosphofructo-2-kinase/fructose-2,6-bisphosphatase 3 (PFKFB3). Co-immunoprecipitation was employed to demonstrate that PFKFB3 ubiquitinated by fizzy and cell division cycle 20 related 1 E3 ligase and was then recognized by P62 autophagy receptor for degradation. Notably, increased PFKFB3 expression was detected both in patients with CD and DSS-induced colitis. Inhibiting PFKFB3 enzyme activity relieved DSS-induced intestinal inflammation and intestinal epithelial barrier damage. The present study proposed a combined therapy targeting autophagy and glycolysis might become a new choice for clinical treatment of IBD.

Correspondence to: Professor Weidong Xiao, General Surgery Laboratory, Department of General Surgery, Xinqiao Hospital, Army Medical University, 183 Xinqiaozhengjie, Shapingba, Chongqing 400037, P.R. China
E-mail: xiaoweidong@tmmu.edu.cn

Professor Min Yu, General Surgery Laboratory, Department of General Surgery, Chongqing General Hospital, Chongqing University, 118 Xingguang Avenue, Liangjiang New Area, Chongqing 401147, P.R. China
E-mail: yumimianbao@163.com

*Contributed equally

Abbreviations: IBD, inflammatory bowel disease; CD, Crohn's disease; IECs, intestinal epithelial cells; PFKFB3, 6-phosphofructo-2-kinase/fructose-2,6-bisphosphatase 3; DSS, dextran sulfate sodium salt; 2-NBDG, 2-deoxy-2-[(7-nitro-2,1,3-benzoxadiazol-4-yl) amino]-D-glucose; PFK-1, phosphofructokinase-1; FZR1/Cdh1, Fizzy and cell division cycle 20 related 1; Baf A1, bafilomycin A1; HK2, hexokinase 2; PKM2, phosphofructokinase, muscle 2; LDHA, lactate dehydrogenase A; PFKP, phosphofructokinase, platelet; CHX, cycloheximide

Key words: inflammatory bowel disease, autophagy, glycolysis, PFKFB3, ubiquitination

Introduction

Inflammatory bowel disease (IBD), including Crohn's disease (CD) and ulcerative colitis, is a chronic idiopathic inflammatory disease of gastrointestinal tract with unknown etiology and recurrent episodes (1). IBD might be the result of a complex interaction between genetic susceptibility, environmental factors and intestinal microflora (2). Autophagy is a conserved cellular process that delivers cytoplasmic material and organelles to lysosomes for breakdown, which plays a key role for cellular renovation and homeostasis (3). A number of studies have also shown that autophagy is involved in regulation of IBD. Impaired autophagy leads to impaired protection against intestinal infection, abnormal Paneth cells morphology, inhibition of intestinal stem cells proliferation and accelerated intestinal epithelial cells (IECs) apoptosis (4). Autophagy related gene 7 knockdown in mice decreases intestinal tight junction proteins levels, exacerbating inflammation of intestinal tract (5). Moreover, knockdown of ATG16L1, a gene associated with autophagy, enhances inflammation and accelerates epithelial cells death in mice (6). In addition, promoting IECs autophagy alleviates colitis in mice (7).

Metabolism provides energy and biomass for maintaining cellular function and proliferation. IECs use oxidative phosphorylation to meet metabolism demand generally. The impaired mitochondrial function in IBD leads to a shift in IECs energy metabolism from oxidative phosphorylation to glycolysis (8-10). Increased glycolysis levels are observed in the colonic epithelium in patients with IBD (11,12). Meanwhile, the metabolomics analysis of mouse colitis model showed

that the level of lactic acid, a metabolite of glycolysis, was increased (13). Inhibition of IECs glycolysis could alleviate colitis in mice and recover intestinal barrier function (14,15).

In the present study, impaired autophagy and abnormal glycolysis levels were observed in the colonic IECs of DSS-induced colitis mice and TNF-α treated NCM460 cells. Subsequently, it demonstrated that autophagy negatively regulated the glycolysis of intestinal epithelial cells by ubiquitin-mediated selective degradation of the key glycolytic enzyme 6-phosphofructo-2-kinase/fructose-2,6-bisphosphatase 3 (PFKFB3). Furthermore, inhibition of PFKFB3 enzyme activity relieved DSS induced intestinal inflammation and intestinal epithelial barrier damage.

Materials and methods

Antibodies and reagents. All antibodies were used at a dilution of 1:1,000 unless otherwise indicated. The antibodies were: Anti-Flag (cat. no. 20543-1-AP), anti-β-actin (cat. no. 20536-1-AP), anti-P62/SQSTM1 (cat. no. 18420-1-AP), anti-occludin (cat. no. 27260-1-AP), anti-claudin-1 (cat. no. 13050-1-AP), anti-fizzy and cell division cycle 20 related 1 (FZR1/Cdh1) (cat. no. 16368-1-AP), anti-claudin-2 (cat. no. 26912-1-AP) from Proteintech Group, Inc.; anti-LC3B (cat. no. 2775S), anti-E-cadherin (cat. no. 14472S) from Cell Signaling Technology, Inc.; anti-ATG7 (WL02793), anti-phosphofructokinase, muscle 2 (PKM2; cat. no. WL03290) from Wanleibio Co., Ltd.; anti-PFKP (cat. no. HA500472) from HUABIO; anti-hexokinase 2 (HK2; cat. no. CQA9312) from Cohesion Biosciences; anti-lactate dehydrogenase (LDHA; cat. no. ab52488) and anti-PFKFB3 (cat. no. ab181861) from Abcam; anti-GAPDH (cat. no. TA310153) from OriGene Technologies, Inc.; anti-Claudin-5 (cat. no. AF5216) from Affinity Biosciences; anti-Claudin-8 (cat. no. GTX77832) from GeneTex, Inc.; anti-K48-linkage specific ubiquitin (cat. no. bsm-63005R) and anti-K63-linkage specific ubiquitin (cat. no. bsm-63006R) from BIOSS. Glucose Content Assay Kit (cat. no. BC2505), Lactic Acid (LA) Content Assay Kit (cat. no. BC2235), Phosphofructokinase (PFK) Activity Assay Kit (cat. no. BC0535) and 2',7'-bis(carboxyethyl)-5(6)-carboxyfluorescein (BCECF; cat. no. IB1750) were purchased from Beijing Solarbio Science & Technology Co., Ltd.. PFKFB3 inhibitor PFK15 (cat. no. S7289), autophagy agonists Rapamycin (cat. no. S1039), autophagy inhibitor Bafilomycin A1 (Baf-A1; cat. no. (S1413) was purchased from Selleck Chemicals. TNF-α (HY-P70426A) was purchased from MedChemExpress. 2-NBDG (cat. no. 72987) was purchased from MilliporeSigma. Fetal bovine serum and DMEM were purchased from Sangon Biotech Co., Ltd.

Animal models. A total of 50 C57BL/6 mice (male, 6-8 weeks old and 23-26 g) were purchased from the Experiment Animal Center (Third Military Medical University, Chongqing, China) for use in the *in vivo* experiments. The C57BL/6 mice were housed under controlled environmental conditions with a temperature of 26˚C, relative humidity of 60% and a 12-h light/dark cycle. Acute colitis was induced by administration of 2.5% dextran sulphate sodium (DSS), which was dissolved in the animals' drinking water, for 7 days. Chronic colitis was induced by administration of 2% DSS, which was dissolved in the drinking water for 21 days. Control mice were provided with distilled water. PFK15 (25 mg/kg) was administered by intraperitoneal injection daily, beginning on the first day of DSS administration. Body weight and stool blood were monitored and recorded every day during DSS feeding. All mice were anesthetized via continuous inhalation of 5% isoflurane for 2 min prior to euthanasia by cervical dislocation. All animal experiments were conducted in accordance with institutional guidelines and approved by the Laboratory Animal Welfare and Ethics Committee of the Third Military Medical University (approval no. AMUWEC20224496).

IEC isolation. The whole colon intestine was removed and placed in tissue culture medium (RPMI 1640, with 10% fetal bovine serum; Sangon Biotech Co., Ltd.). The section was cut into 5-mm pieces, washed in an isolation buffer containing 190 mg ethylenediaminetetraacetic acid and 80 mg Dithiothreitol (DTT) dissolved in phosphate-buffered saline (PBS) 500 ml and incubated in the same buffer with continuous brisk stirring at 37˚C for 30 min. The supernatant was filtered rapidly through 70 and 30 μm filter screen. Following centrifugation at 600 x g for 5 min at 37˚C, the cells recovered in the suspension were collected for RNA or protein extraction. Intestinal epithelial cell isolation was used for western blotting and reverse transcription-quantitative (RT-q) PCR.

Cell culture and transfection. The normal intestinal epithelium cell line NCM460 was purchased from the American Type Culture Collection (ATCCSA). Cells were cultured in Dulbecco's modified Eagle's medium (DMEM) supplemented with 10% fetal bovine serum (FBS), 1% Penicillin-streptomycin solution. The dry powder small interfering (si)RNA was dissolved in sterile, nuclease-free water (cat. no. R1600; Beijing Solarbio Science & Technology Co., Ltd.) to a concentration of 20 μM. Cell transfection with siRNA was performed following the manufacturer's instructions for the riboFECT CP (cat. no. C10502-05; Guangzhou RiboBio Co., Ltd.) Transfection Kit. The procedure is outlined as follows: Seed $5x10^5$ cells into 6-well plates, then prepare a transfection mixture by combining 100 μl of transfection buffer, 100 nM siRNA, and 12 μl of transfection reagent. Incubate the mixture at 25˚C for 15 min before adding it to the cells. After 12 h of co-incubation of the cells with the mixture, replace the culture medium. Following medium replacement, continue culturing the cells for an additional 48 h, and then evaluate the gene silencing effect using qPCR and western blotting. The negative control siRNA is transfected into the cells using an identical transfection protocol. The siRNA was constructed by Sangon Biotech Co., Ltd. The siRNA used were: siPFKFB3 no.1 sense: (5'-CGUGUCGGUUCCAUUCCAUUU-3'); siPFKFB3 no.2 sense: (5'-ACCCGCUCAUGAGACGCAAUA-3'); siPFKFB3 no.3 sense: (5'-GGGACUUGUCGCUGAUCAAGG-3'); siATG7 sense: (5'- CCCAGCUAUUGGAACACUGUA-3'); negative control siRNA sense: (5'-UUCUCCGAACGUGUCACGU-3').

Short hairpin (sh)RNA and siRNA. For stable ATG7 siRNA, PFKFB3 siRNA, FZR1 siRNA expression, the retroviral encoding hairpin RNA sequences were constructed. shRNA sequence against ATG7, PFKFB3, FZR1 were generated and cloned into the expression vector. Recombinant lentiviruses

expressing GFP-tagged shATG7, shPFKFB3 were constructed by Sangon Biotech Co., Ltd. The lentiviral expressing shFZR1, PFKFB3(NM_004566)-PCDH-PURO-3XFlag, SQSTM1(NM_003900)-PCDH-PURO-3XFlag and FZR1 (NM_001136198)-PCDH-GFP+PURO-3XFlag were constructed by YouBio. psPAX2 (cat no. VT1444) and pMD2.G (cat no. VT1443) were purchased from YouBio. Polyethylenimine (PEI) (cat no. 306185) was purchased from MilliporeSigma. The 293T cell line (cat no. CL-0005) was obtained from Procell and used in experiments after culture for at least three generations. The transfection reagents were prepared in advance as follows: A solution (psPAX2 8.34 μg, pMD2.G 2.52 μg, DMEM 481.1 μl); B solution (lentiviral plasmid 8.04 μg, PEI 59.7 μg, DMEM 440.3 μl). The A solution was mixed with the B solution at room temperature and incubated for 15 min. The mixture was added to a 10 cm culture dish containing 293T cells at 60-70% confluence, and incubated at 37˚C for 12 h. The supernatant was removed and the cells washed twice with PBS and 10 ml of complete DMEM medium added. Culture was continued at 37˚C for an additional 48 h. The supernatant was collected and transferred it into a 15 ml centrifuge tube then centrifuged at 200 x g and 25˚C for 5 min. Concurrently, the supernatant was filtered through a 0.45 μm pore-size filter membrane (cat no. SLHVM33RS; MilliporeSigma). The viral stock solution was concentrated with 100 kDa Millipore ultrafiltration tubes (cat no. UFC9100; MilliporeSigma) and stored at -80˚C. Concentrated viruses (10 MOI) were used to infect $5x10^5$ cells in a 6 cm dish. Infected cells underwent sorting by 2 μg/ml puromycin for 48 h for stably target expression. The shRNA used were: shATG7 (5'-CCCAGCTATTGGAACACTGTA-3'); shPFKFB3 no.1 (5'-CGTGTCGGTTCCATTCCATTT-3'); shPFKFB3 no.2 (5'-ACCCGCTCATGAGACGCAATA-3'); shPFKFB3 no.3 (5'-GGGACTTGTCGCTGATCAAGG-3'); shFZR1 (5'-GTGAACTTCCACAGGATTAAC-3')

Metabolite measurements. Glucose content in cell was measured using colorimetric kits (cat. no. BC2505; Beijing Solarbio Science & Technology Co.,Ltd.) and lactic acid content in the culture supernatants was measured using colorimetric kits (cat. no. BC2235; Beijing Solarbio Science & Technology Co., Ltd.) according to the manufacturer's instructions. The absorbance of glucose was measured at 505 nm and lactic acid was measured at 570 nm using a SpectraMax M2 microplate reader (Molecular Devices, LLC). Phosphofructokinase (PFK) activity in cell was measured using colorimetric kits (cat. no. BC0535; Beijing Solarbio Science & Technology Co., Ltd.) according to the manufacturer's instructions. The absorbance of phosphofructokinase-1 (PFK-1) was measured at 340 nm using a SpectraMax M2 microplate reader (Molecular Devices, LLC). All experiments were performed in triplicate as described previously.

RT-qPCR. Total cellular RNA was extracted from $5x10^5$ cells in a 6 cm dish with RNAiso Plus (Takara Bio, Inc.) and used the Advantage RT-for-PCR Kit (Takara Bio, Inc.) for reverse transcription. The procedure was performed as follows: First, RNAiso Plus (1 ml) was added to the cell pellet to ensure complete cell lysis. Next, 200 μl of chloroform was added, mixed thoroughly and centrifuged at 15,000 x g for 15 min at 4˚C. Then, transfer the aqueous phase and mix with an equal volume of isopropanol to precipitate RNA, followed by centrifugation at 15,000 x g for 10 min at 4˚C. After centrifugation, the supernatant was carefully discarded and the RNA pellet washed twice with absolute ethyl alcohol to remove impurities. Finally, the pellet was briefly air-dried to remove residual ethanol and the resulting white precipitate dissolved in RNase-free water. The purified material represented the total RNA extracted from the cells. RNA was converted into cDNA through reverse transcription reaction on the Applied Biosystems thermal cycler (Thermo Fisher Scientific, Inc.). The reverse transcription reaction was performed as follows: Incubation at 37˚C for 15 min, followed by enzyme inactivation at 85˚C for 5 sec and storage at 4˚C for 10 min. qPCR was performed using the SYBRPrime qPCR kit (cat. no. BG0014; BioGround Corp.) under the following conditions: Initial pre-denaturation at 94˚C for 20 sec, followed by 40 cycles of denaturation at 94˚C for 10 sec and annealing and extension at 60˚C for 30 sec. Relative quantitation of all transcripts was calculated using the comparative Ct method with β-actin as an internal control (16). This assay was performed in triplicate. The primers used for detection are in Table I.

Table I. Primers used in quantitative PCR.

Gene	Sequence
PFKP	F: 5'-GGAGTGGAGTGGGCTGCTGGAG-3'
	R: 5'-CATGTCGGTGCCGCAGAAATCA-3'
LDHA	F: 5'-ATGGCAACTCTAAAGGATCAGC-3'
	R: 5'-CCAACCCCAACAACTGTAATCT-3'
HK2	F: 5'-CATCCAGAGGAGAGGGGACT-3'
	R: 5'-TCATCGCCTTCCACCATGTC-3'
PKM2	F: 5'-CTGTGGACTTGCCTGCTGTG-3'
	R: 5'-TGCCTTGCGGATGAATGACG-3'
PFKFB3	F: 5'-CAGTTGTGGCCTCCAATATC-3'
	R: 5'-GGCTTCATAGCAACTGATCC-3'
GAPDH	F: 5'-CCTTCCGTGTCCCCACT-3'
	R: 5'-GCCTGCTTCACCACCTTC-3'
ATG7	F: 5'-GTTGTTTGCTTCCGTGAC-3'
	R: 5'-TGCCTCCTTTCTGGTTCT-3'
IL-1β	F: 5'-AGTTGACGGACCCCAAA-3'
	R: 5'-TCTTGTTGATGTGCTGCTG-3'
IL-6	F: 5'-ACAGAAGGAGTGGCTAAGGA-3'
	R: 5'-AGGCATAACGCACTAGGTTT-3'
TNF-α	F: 5'-CCACCACGCTCTTCTGTCTACTG-3'
	R: 5'-GGGCTACGGGCTTGTCACTC-3'

Immunoblot and immunoprecipitation. For immunoblotting, $5x10^6$ Cells were lysed by 300 μl RIPA buffer (cat. no. R0020; Beijing Solarbio Science & Technology Co., Ltd.) supplemented with 3 μl protease inhibitor cocktail (cat. no. P0100-01; Beijing Solarbio Science & Technology Co., Ltd.) for 30 min at 4˚C. Then, it was centrifuged at 4˚C and 12,000 x g for 10 min. The protein was denatured by adding 5X SDS loading buffer and boiled at 100˚C for 10 min, then separated by sodium dodecyl-sulfate polyacrylamide gel

electrophoresis (SDS-PAGE). β-actin antibody and the target protein antibody were diluted separately in primary antibody dilution buffer (cat no. C1240; Applygen) at 1:1,000, followed by overnight incubation at 4˚C. On the following day, the goat anti-rabbit IgG secondary antibody (cat no. BA1056; Wuhan Boster Biological Technology, Ltd.) was diluted in secondary antibody diluent buffer (cat no. C1241; Applygen) at 1:5,000 and incubated at 37˚C for 1 h before being washed three times with PBST buffer, 5 min per wash. The PBST solution was prepared by adding 500 μl of Tween 20 to 500 ml of phosphate-buffered saline (PBS). Immunodetection was performed by enhanced chemiluminescence (ECL System; Azure Biosystems, Inc.). For immunoprecipitation assays, the cells were washed and collected with cold PBS from 10 cm dish. Cells were collected into a 1.5 ml Eppendorf (EP) tube (cat no. FTUB015; Beyotime Biotechnology) and placed the tube on ice for pre-cooling. Freshly prepared 0.3% IP lysis buffer (1 ml) containing protease inhibitor cocktail was added, mixed gently by inverting or pipetting and incubated at 4˚C on a rotating mixer for 60 min at a moderate to slightly increased rotation speed. After completed lysis, the EP tube was kept on ice and followed by ultrasonic homogenization using the following settings: 20% amplitude, 1-sec pulse duration, 1-sec interval, for a total of 30 cycles. Subsequently, the sample was centrifuged at 4˚C and 15,000 x g for 10 min. The supernatant was carefully collected without disturbing the pellet and transferred to a new pre-chilled EP tube. A total of 300 μl of the supernatant was taken as the Input sample, 75 μl of 5X Loading Buffer added and mixed thoroughly and boiled in a water bath at 100˚C for 10 min. The sample was immediately transferred to -80˚C for long-term storage. The remaining supernatant was divided equally into two portions, which were then incubated overnight at 4˚C on a rotator with either the target primary antibody (2 μg) or the immunoglobin G (IgG) control antibody (1 μl), respectively. The following day, 30 μl of Protein A/G magnetic bead suspension was added to each tube and incubated with rotation at 4˚C for 4 h. After incubation, the tubes were placed on a magnetic stand to immobilize the beads, then carefully aspirated the supernatant. The beads were washed by adding 1 ml of 0.1% IP lysis buffer to each tube, followed by rotating incubation at a slightly increased speed for 5 min. The washing procedure was repeated five times. After the final wash the was complete removal of residual liquid. Subsequently, 20 μl of 2X loading buffer was added to each tube to thoroughly resuspend the magnetic beads, the samples boiled at 100˚C for 10 min, and immediately transferred to -80˚C for storage until further use for western blot analysis. The IP lysis buffer was prepared by mixing 10% NP-40, 1 M Tris-HCl, 5 M NaCl, 0.5 M EDTA, and deionized water (ddH_2O) to final concentrations in accordance with standard immunoprecipitation protocols.

Detection of protein stability by the cycloheximide (CHX). NCM460 cells were treated with 100 μg/ml CHX alone or in combination with 200 nM rapamycin. Cell samples were collected at indicated time points (0, 3, 6, 9, 12, and 24 h), and the expression levels of the target protein were analyzed by western blotting. The resulting data were fitted to a linear regression model to calculate the half-life of the target protein in NCM460 cells.

Analysis of autophagic flux. The viral infection of cells was performed according to the instructions provided in the adenovirus user manual. When the cells in 50 mm dish reached a density of ~30%, 1 μl of mRFP-GFP-LC3 adenovirus (cat no. GENE-497, Shanghai GeneChem Co., Ltd.) ($1x10^{11}$ PFU/ml) was added to each well for transfection. The dish was then incubated at 37˚C for 24 h. Then cells were cultured for 24 h with or without TNF-α. The images were acquired using an inverted fluorescence microscope (Olympus Corporation). Yellow (merge of GFP signal and RFP signal) puncta represented early autophagosomes, while red (RFP signal) puncta indicated late autolysosomes. Autophagic flux was evaluated by the change of yellow puncta/red puncta.

Glucose uptake assay. Cells were treated with bafilomycin A1 (Baf A1), Rapamycin, TNF-α or transfected with siATG7. The DMEM culture medium was replaced by glucose-free medium for 2 h. 2-NBDG was added at a concentration of 100 μM for 30 min. Then, cells were washed by PBS twice. The images were acquired using an inverted fluorescence microscope (Olympus Corporation). The fluorescence intensity of 2-NBDG was detected at λex 494 nm, λem 551 nm by using a SpectraMax M2 microplate reader (Molecular Devices, LLC).

Determination of intracellular pH. The intracellular pH was detected by fluorescence measurements using the dye BCECF-AM (Beijing Solarbio Science & Technology Co., Ltd.). Cells grown in 96-well microtiter plate were washed with PBS for twice and incubated with 3 μM BCECF-AM for 30 min at 37˚C. The medium of cells was removed and cells were washed twice with PBS. The images were acquired using an inverted fluorescence microscope (Olympus Corporation). The fluorescence intensity of BCECF-AM was detected at λex 488 nm, λem 535 nm by using a SpectraMax M2 microplate reader (Molecular Devices, LLC).

Immunohistochemistry and immunofluorescence. Samples were fixed in 4% paraformaldehyde (Beijing Solarbio Science & Technology Co., Ltd.) at 4˚C overnight. The fixed tissues were sequentially immersed in 50, 70, 85, 95 and 100% ethanol solutions for 90 min each to achieve gradual dehydration to ensure complete water removal. The tissue was immersed in a 1:1 mixture of ethanol and xylene for 60 min, followed by immersion in pure xylene for an additional 60 min. Subsequently, the tissue was transferred to a 1:1 mixture of xylene and paraffin for 60 min, then placed in pure paraffin solution for 120 min. Finally, the tissue was incubated in molten paraffin at 62˚C for 2 h to ensure complete infiltration of the colon tissue. The colon tissue was placed in a mold and molten paraffin was added. After waiting for the paraffin to solidify, the tissue wax blocks were cut into thin slices ~3 μm thick using a microtome. The immunohistochemical sections were incubated with the PFKFB3 primary antibody overnight at 4˚C, followed by incubation with the anti-rabbit secondary antibody at 37˚C for 1 h. The immunofluorescence sections were incubated overnight at 4˚C with the primary antibodies against PFKFB3 and E-cadherin, followed by incubation at 37˚C for 1 h with Alexa Fluor 488-conjugated and Alexa Fluor 555-conjugated secondary antibodies in the dark. The cell nuclei were stained with DAPI at a temperature of 37˚C for

10 min. Images were acquired by using fluorescence microscopy (Olympus Corporation). A total of 19 blood samples from patients with Crohn's disease and 21 blood samples from healthy individuals were collected. Additionally, five colon tissue samples were obtained from patients with Crohn's disease. The male-to-female ratio across all patient samples was ~2:1, with an age range of 22-50 years. All human tissue were collected using protocols approved by Medical Ethics Committee of Second Affiliated Hospital of Army Medical University, PLA and informed consent had been obtained from the patients (approval no. 2022-188-01).

Statistical analysis. Crohn's disease datasets were downloaded from http://www.ncbi.nlm.nih.gov/geo. High-throughput transcriptome data from blood samples of healthy individuals and IBD patients, retrieved from the GEO database (accession numbers GSE119600, GSE112057 and GSE126124), were analyzed to mRNA expression of the PFKFB3 between the two groups. The ubiquitin ligase associated with the PFKFB3 protein was predicted and analyzed using the http://ubibrowser.ncpsb.org.cn. Statistical analyses of all data were performed using GraphPad Prism (version 8.0; Dotmatics). Comparisons between two groups were analyzed by a two-tailed, unpaired Student's t-test. One-way ANOVA followed by Tukey's post-hoc test was used for multiple comparisons Data from at least three independent experiments unless otherwise noted. Error bars represent SEM and statistical significance is indicated as $^{*}P<0.05$, $^{**}P<0.01$, $^{***}P<0.001$, $^{****}P<0.0001$. $P<0.05$ was considered to indicate a statistically significant difference.

Results

Impaired autophagy and elevated glycolysis levels in IBD. First, to elucidate the changes of autophagy in IBD, acute and chronic colitis models were established in C57BL/6 mice. DSS concentration of 2.5% (w/vol) in the drinking water for 7 days induce marked colitis in C57BL/6 mice. In addition, chronic colitis model was induced in C57BL/6 mice by three cycles of 2% DSS (7 days of DSS induction, 14 days water) (Fig. 1A). The present study extracted the colonic epithelial cells of colitis mice and detected the expression of autophagy marker proteins (P62 and LC3b) by western blotting. As shown in Fig. 1B, the expression of P62 and LC3b were markedly increased in colonic epithelial cells of acute and chronic colitis mice. The mRNA levels of key glycolysis enzymes were detected to explore the glycolysis levels. PCR data showed that the expression levels of PFKP, LDHA and PFKFB3 were markedly increased in DSS group (Fig. 1C). However, the mRNA levels of HK2 and PKM2 were decreased in DSS group (Fig. 1C).

Meanwhile, TNF-α (200 ng/ml) was used to induce inflammation in NCM460, one of the human IECs lines. Autophagic flux was detected by transfecting mRFP-GFP-LC3 double fluorescence adenovirus in IECs. Autophagosome with double limiting membrane structure was marked by both mRFP and GFP, which appeared as yellow puncta. GFP fluorescent protein was known to quench under acidic conditions. Therefore, autolysosomes with low pH were marked by only mRFP which appeared as red puncta. Quantification of LC3 puncta number of representative cells is shown in Fig. 1D. Compared with the control group, the number of autophagosomes in the TNF-α group increased while the number of autolysosomes decreased. This suggested that the process of fusion of autophagosome and lysosome was blocked in inflammatory IECs and the accumulation of autophagosome occurred in inflammatory IECs. *In vivo* and *in vitro* models of colitis both suggested impaired autophagy of colon epithelial cells under inflammation. Subsequently, the glycolysis levels in model of inflammatory IECs was further investigated. Intracellular glucose content and lactic acid production were measured in TNF-α induced IECs. Glucose content decreased markedly and lactic acid production increased in inflammatory IECs, suggesting an enhanced glycolysis level (Fig. 1E). A 2-deoxy-2-[(7-nitro-2,1,3-benzoxadiazol-4-yl) amino]-D-glucose (2-NBDG) fluorescence probe was then used to detect the rate of glucose uptake in IECs (Fig. 1F) and a pH-sensitive dye 2',7'-Bis(2-carboxyethyl)-5(6)-carboxy-fluorescein BCECF fluorescence probe to detect intracellular acidity (Fig. 1G). It was known that 2-NBDG fluorescence density increased with the increased of cellular glucose uptake rate, while BCECF fluorescence density increases with the decreased of pH in IECs. Quantitative statistics of fluorescence density showed that the density of 2-NBDG and BCECF markedly increased in inflammatory IECs, suggesting that inflammatory stimulation resulted in increasing glucose uptake rate and cell acidity. These data indicated that the level of glycolysis was increased under inflammation.

Autophagy negatively regulates glycolysis in intestinal epithelial cells. Autophagy-related genes (ATGs) are core conserved genes that coordinate and mediate the formation of the double membrane structure of autophagosomes in eukaryotic cells and transfer the contents of cytoplasm to lysosome degradation (17). ATG7 protein encoded by autophagy-related genes participates in the lipidation process of autophagosome formation, driving phosphatidylethanolamine (PE) to bind to LC3-I to generate LC3-II which promotes autophagy. ATG7 impairment classically results in autophagy defects in cells and tissues (18). The present study stably expressed retrovirus shRNA against ATG7 in IECs (Fig. 2A). In ATG7 knock-down cells, glucose content decreased while lactate production increased (Fig. 2B). In addition, increased rate of glucose uptake (Fig. 2C) and intracellular acidity (Fig. 2D) were observed in ATG7 knockdown cells. Furthermore, the enzyme activity of PFK-1, one of the key rate-limiting enzymes in glycolysis was detected and it was found that PFK-1 activity was enhanced in ATG7 knockdown cells (Fig. 2E). This might be related to the increased rate of glycolysis. Taken together, these data suggested that impaired autophagy caused by ATG7 knockdown in IECs lead to increased glycolysis levels.

Subsequently, to further elucidate the regulation of autophagy on glycolysis, IECs was treated by autophagy activator rapamycin, or the autophagy inhibitor Baf A1. Glucose content and lactate production were measured in rapamycin or Baf A1 treated IECs (Fig. 3A and B). Data showed that activation of autophagy inhibited the production of glycolytic metabolites and reduced glycolysis level. Furthermore, increased rate of glucose uptake and intracellular acidity were observed in Baf A1 treated IECs, while decreased rate of glucose uptake and intracellular acidity were observed in rapamycin treated IECs (Fig. 3C and D). Moreover, PFK-1

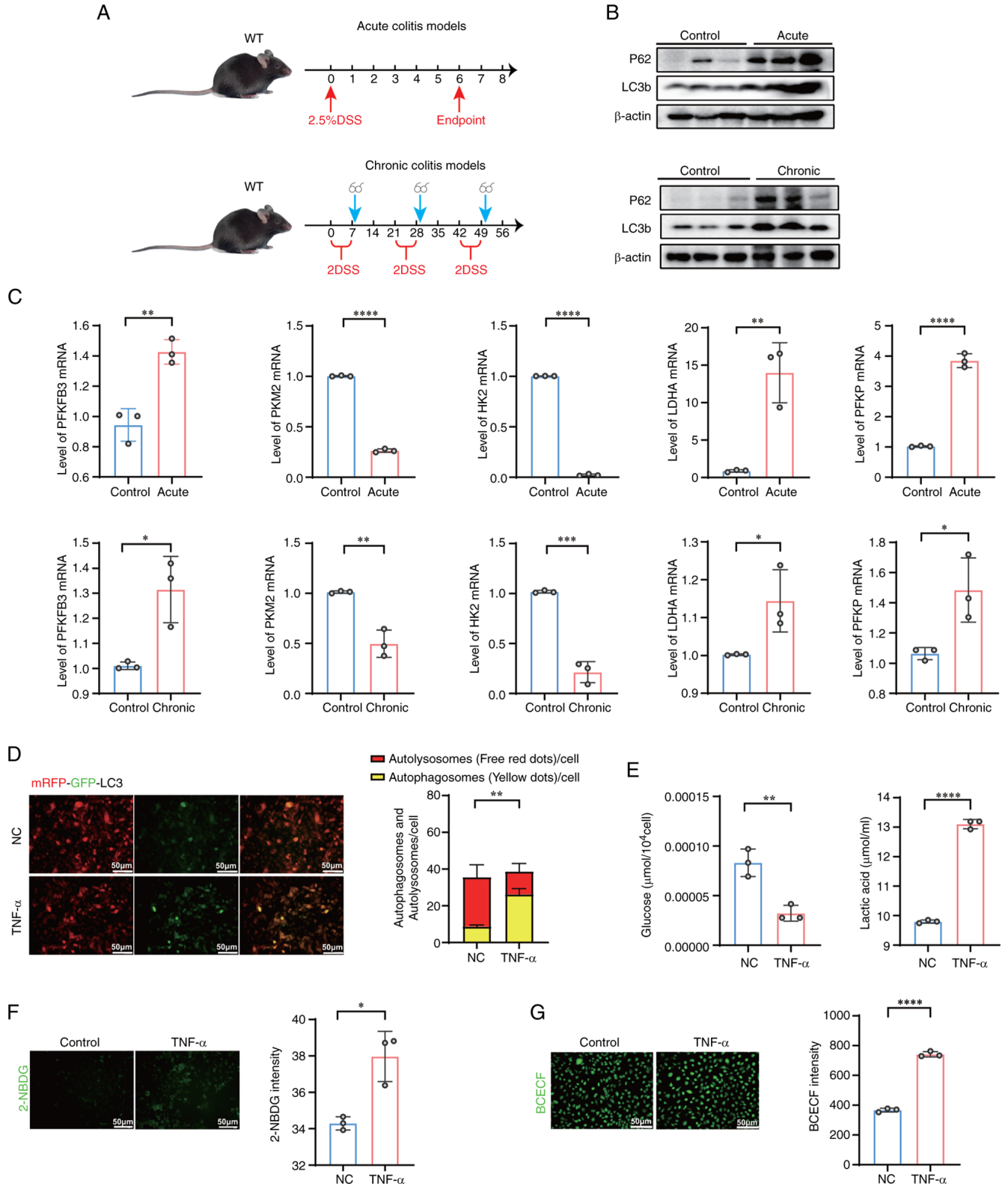

Figure 1. Impaired autophagy and upregulated glycolysis levels in IECs were observed under inflammatory conditions. (A) Establishment of acute colitis mouse model and chronic colitis mouse model. (B) The protein levels of P62 and LC3b in colonic epithelial cells of acute DSS-induced mice (n=3) and chronic DSS-induced mice (n=3) determined by western blot analysis. (C) mRNA levels of PFKP, LDHA, HK2, PKM2, PFKFB3 in DSS-induced mice epithelial cells. (D) Autophagic flux was measured by transfecting cells with mRFP-GFP-LC3 dual-fluorescence adenovirus (Ad-LC3), allowing differentiation between autophagosomes (mRFP+/GFP+ fluorescence, appearing as yellow puncta) and autolysosomes (mRFP+/GFP- fluorescence, appearing as red puncta). TNF-α (200 ng/ml) induced epithelial cells for 48 h. Representative immunofluorescence images were shown. (Original magnification, x20). Quantification of LC3 puncta number of representative cells. (E) Relative glucose content and lactate (Lac) production in control vs. TNF-α induced epithelial cells. (F) 2-NBDG and (G) BCECF fluorescent counter-staining in TNF-α induced epithelial cells vs. control. Representative immunofluorescence images were shown. (Original magnification, x20). Quantitative fluorescence intensity of 2-NBDG and BCECF (n=3). Data were presented as the mean ± SD of n=3 per group. Statistical analysis was performed using unpaired t-tests. ****P<0.0001, ***P<0.001, **P<0.01, *P<0.05, ns, non-significant vs. control group. IECs, intestinal epithelial cells; DSS, dextran sulfate sodium salt; 2-NBDG, 2-deoxy-2-[(7-nitro-2,1,3-benzoxadiazol-4-yl) amino]-D-glucose; BCECF, 2',7'-bis(carboxyethyl)-5(6)-carboxy-fluorescein.

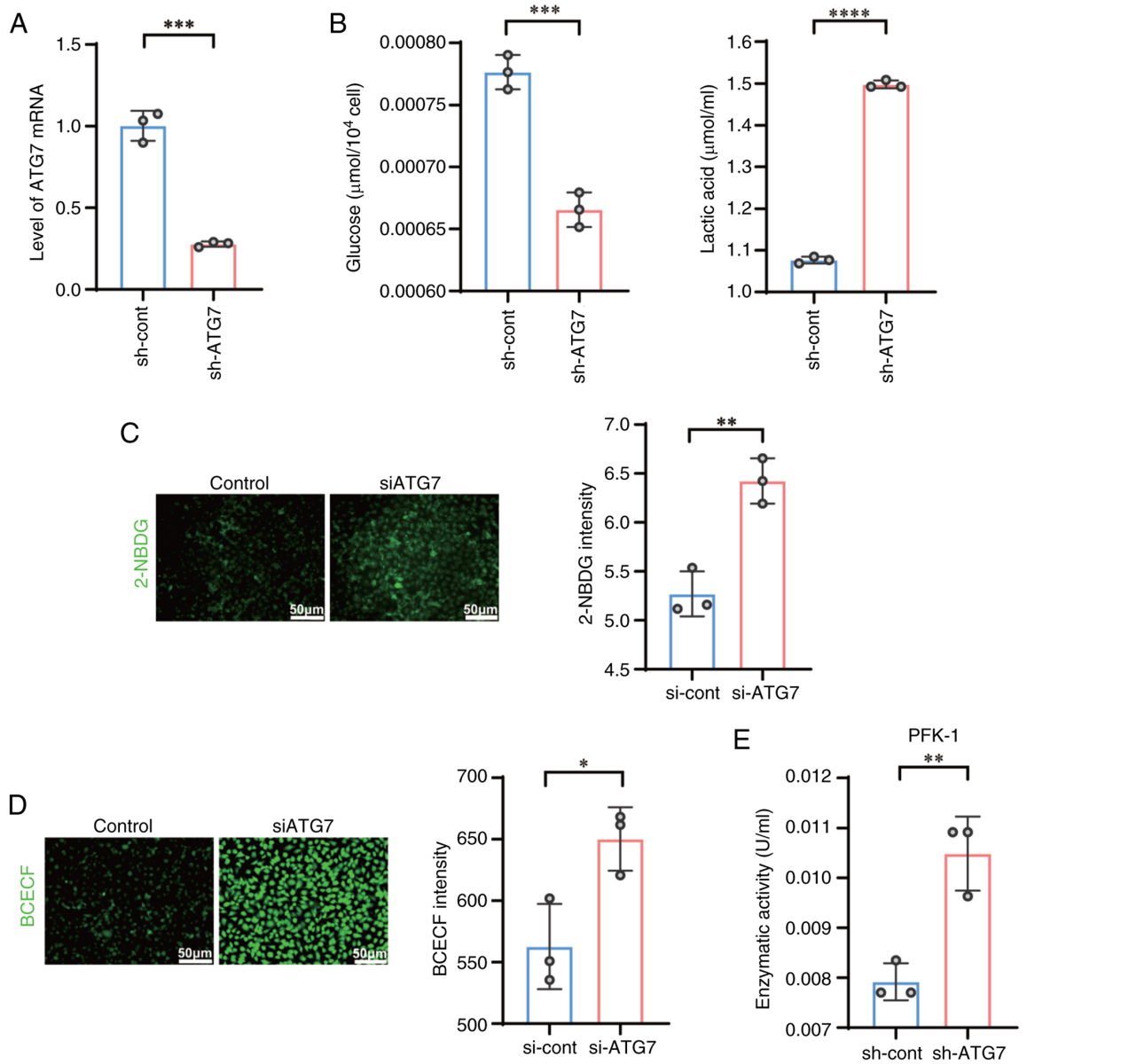

Figure 2. Knockdown of ATG7 in IECs resulted in increased glycolysis levels. (A) mRNA levels of ATG7 in control vs. sh-ATG7 epithelial cells. (B) Relative glucose content and lactate (Lac) production in control vs. sh-ATG7 epithelial cells. (C) 2-NBDG and (D) BCECF fluorescent counter-staining in ATG7 knockdown epithelial cells vs. control. Representative immunofluorescence images were shown. (Original magnification, x20). Quantitative fluorescence intensity of 2-NBDG and BCECF. (E) Enzymatic activities of PFK-1 in ATG7-knockdown epithelial cells vs. control (n=3). P-values were calculated using an unpaired t-test. The values were presented as the means ± SEM, n=3, *P<0.05, **P<0.01, ***P<0.001, ****P<0.0001. ATG, autophagy related gene; IECs, intestinal epithelial cells; sh, short hairpin; si, small interfering; 2-NBDG, 2-deoxy-2-[(7-nitro-2,1,3-benzoxadiazol-4-yl) amino]-D-glucose; BCECF, 2',7'-bis(carboxyethyl)-5(6)-carboxyfluorescein; PFK-1, phosphofructokinase-1.

enzyme activity was detected in IECs treated with rapamycin or Baf A1 (Fig. 3E). Similar to ATG7 knockdown cells, activation of autophagy negatively regulated PFK-1 enzyme activity. The aforementioned data indicated that activation of autophagy promotes decreased of glycolysis level in IECs and inhibition of autophagy resulted in elevated glycolysis.

PFKFB3 is required for autophagy to regulate glycolysis in IECs. The present study next attempted to identify possible key protein in the process of autophagy regulation of glycolysis. It examined the protein expression levels of six key glycolytic enzymes, HK2, PKM2, LDHA, PFKP, GAPDH and PFKFB3 in control group and autophagy deficient (ATG7 knockdown) cells group. Notably, only PFKFB3 protein levels increased in ATG7 knockdown IECs. There was no significant difference in the protein expression of other key glycolytic enzymes in ATG7 knockdown IECs group and control group (Fig. 4A). Base on aforementioned results, it was next examined whether rapamycin or Baf A1 regulated the protein expression of PFKFB3 in IECs. IECs were treated with different concentrations (50, 100 and 200 nM) of Baf A1 or different concentrations (100, 200 and 400 nM) of rapamycin for 24 h. Meanwhile, IECs were treated with 200 nM Baf A1 or rapamycin for different times (12, 24 and 48 h). Western blotting showed that Baf A1 inhibited autophagy and increased expression of PFKFB3 protein. In contrast to the Baf A1, rapamycin activated autophagy and reduced levels of PFKFB3 protein (Fig. 4B and C).

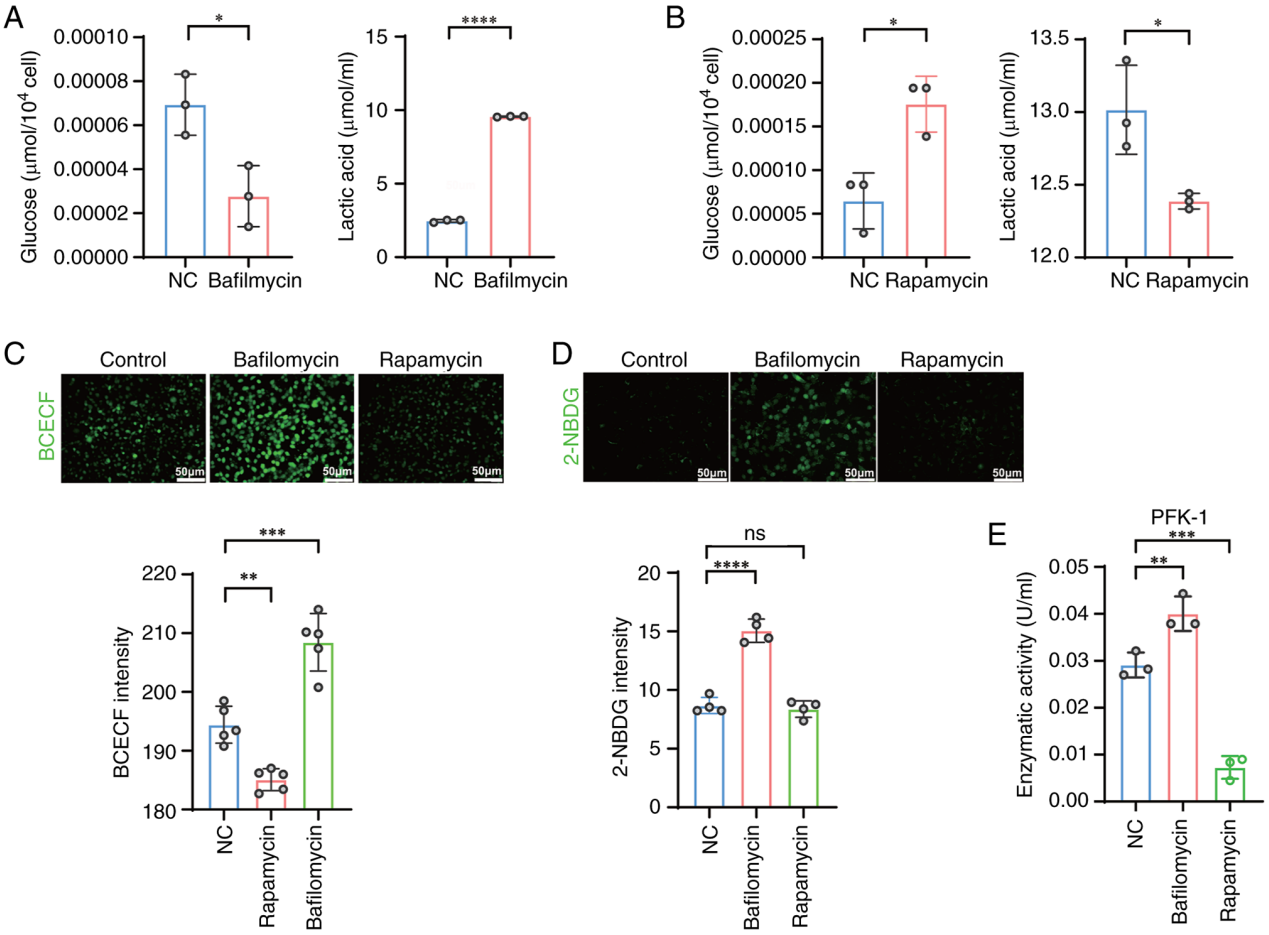

Figure 3. Autophagy agonists and inhibitors regulated glycolysis. (A) Relative glucose content and Lac production in control vs. Baf A1 treated IECs. (B) Relative glucose content and Lac production in control vs. rapamycin treated IECs. (C and D) 2-NBDG and BCECF fluorescent counter-staining in rapamycin or BafA1 treated IECs vs. control. Representative immunofluorescence images were shown. (Original magnification, x20). Quantitative fluorescence intensity of 2-NBDG and BCECF (n=3). (E) Enzymatic activities of PFK-1 in rapamycin or BafA1 treated IECs vs. control (n=3). P-values were calculated using One-way ANOVA followed by Tukey's post-hoc test. The values were presented as the means ± SEM, *P<0.05, **P<0.01, ***P<0.001, ****P<0.0001. Lac, lactate; Baf A1, bafilomycin A1; IECs, intestinal epithelial cells; 2-NBDG, 2-deoxy-2-[(7-nitro-2,1,3-benzoxadiazol-4-yl) amino]-D-glucose; BCECF, 2',7'-bis(carboxyethyl)-5(6)-carboxyfluorescein; PFK-1, phosphofructokinase-1.

To further elucidate the importance of PFKFB3, PFKFB3 knockdown and overexpression intestinal epithelial cells were constructed (Fig. 5A). PFKFB3 knockdown cells were treated with Baf A1 for 24 h. After autophagy was inhibited in PFKFB3 knockdown cells, it was observed that compared with normal epithelial cells treated with Baf A1, the glucose content of PFKFB3 knockdown cells were markedly increased and lactic acid production was decreased (Fig. 5B). Result of 2-NBDG and BCECF, indicated that PFKFB3 knockdown reduced the rate of intracellular glycolysis and impaired the ability of autophagy inhibitors to promote glycolysis (Fig. 5C and D). Moreover, compared with PFKFB3 knockdown cells without rapamycin, the relative glucose content and lactic acid production of PFKFB3 knockdown cells treated with rapamycin were not markedly changed (Fig. 5E). Furthermore, the results of 2-NBDG and BCECF also indicated that rapamycin has no effect on the glycolysis rate following PFKFB3 knockdown (Fig. 5F and G). All of these results indicated that PFKFB3 plays a key role in autophagy regulation of intestinal epithelial cells glycolysis. Subsequently, the role of the autophagy activator rapamycin was validated in PFKFB3-overexpressing NCM460 cells. Overexpression of PFKFB3 increased glucose content and decreased lactic acid production in intestinal epithelial cells following treatment with rapamycin (Fig. 5H). Flag-tagged PFKFB3 overexpression cells had shown high level of 2-NBDG and BCECF, while rapamycin treatment reduced it (Fig. 5I and J). It suggested that PFKFB3 increased in intestinal epithelial cells induced high level of glycolysis, while promoting autophagy can alleviate the level of PFKFB3-induced glycolysis.

P62 specifically targets FZR1/Cdh1 ubiquitination PFKFB3 and mediates its autophagic degradation in IEC. The present authors have previously verified that autophagy can regulate the expression of PFKFB3 protein. Foerster *et al* (4) reported that selective autophagy regulated intestinal environmental homeostasis by degrading specific proteins. This implied that autophagy might regulate PFKFB3 protein stability. To test this hypothesis, NCM460 cells with or without rapamycin were treated with cycloheximide (CHX) to inhibit protein synthesis, followed by monitoring the levels of remaining PFKFB3 at the indicated time points (Fig. 6A). The results indicated that PFKFB3 protein stability was disrupted by rapamycin and the PFKFB3 degradation was mediated by

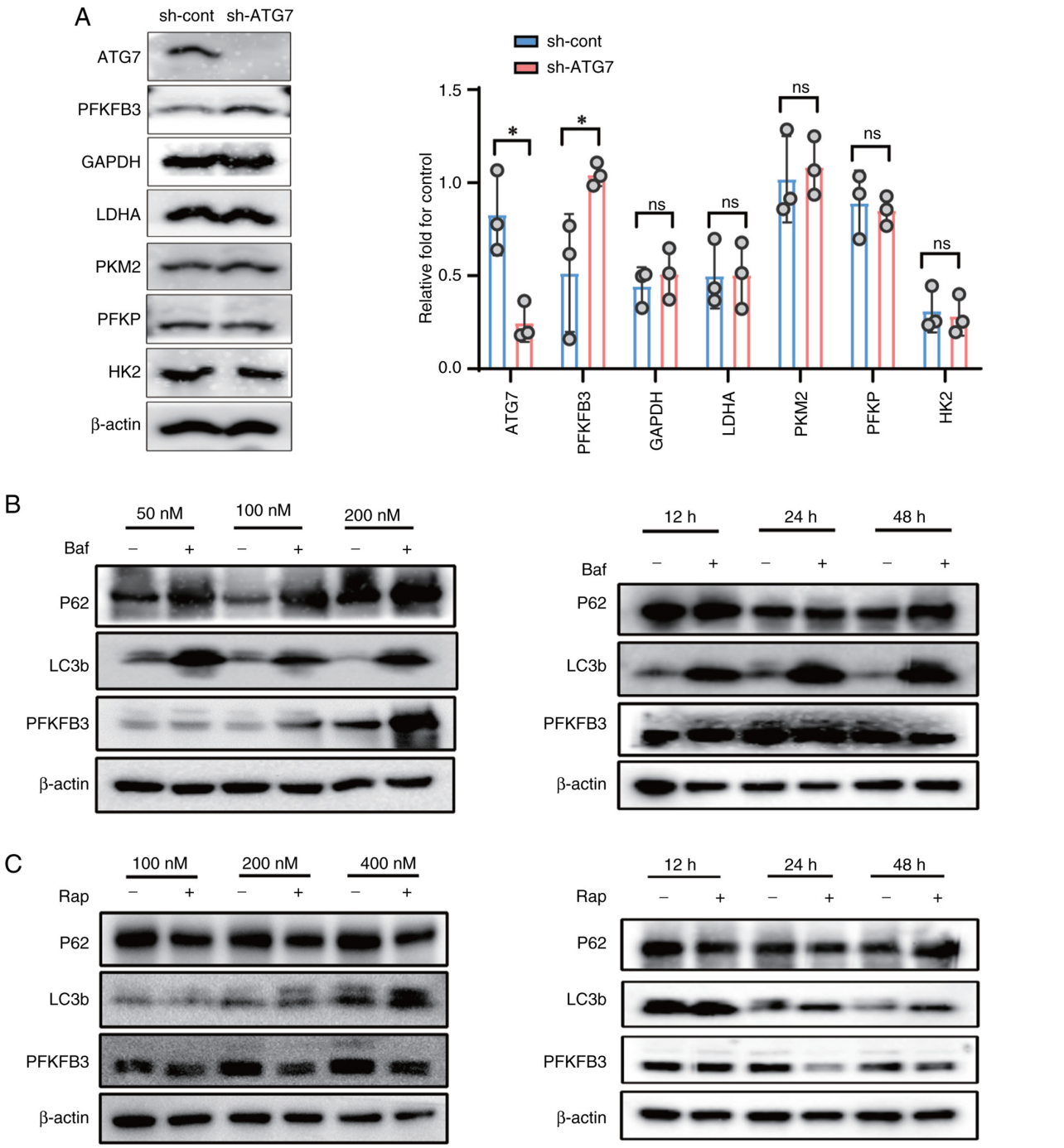

Figure 4. Autophagy regulated glycolysis levels through PFKFB3. (A) Knockdown ATG7 had no effect on the expression levels of genes encoding glycolytic proteins except PFKFB3. Normalized quantification of mean gray intensity was determined from three separate experiments. The values were presented as the means ± SEM. Protein levels of P62, LC3b and PFKFB3 in control vs. (B) rapamycin or (C) Baf A1 treated epithelial cells. P-values were calculated using an unpaired t-test. The values were presented as the means ± SEM, *P<0.05. ns, non-significant. PFKFB3, 6-phosphofructo-2-kinase/fructose-2,6-bisphosphatase 3; ATG, autophagy related gene; Baf A1, bafilomycin A1.

autophagy. Selective autophagy is mediated by autophagy receptors and P62/SQSTM1 is a common autophagy receptor in mammals (19). It was hypothesized that P62 receptor mediated the degradation of PFKFB3 protein in intestinal epithelial cells. First, PFKFB3 and P62 were labelled by immunofluorescence, which showed that PFKFB3 and P62 were co-localized (Fig. 6B). The results indicated that PFKFB3 might interacted with P62. Subsequently, the coimmunoprecipitation assays showed that P62 could interact with PFKFB3, suggesting that P62 played a key role in PFKFB3 degradation (Fig. 6C). To further elucidate the effect of P62 on the degradation of PFKFB3, Flag-tagged P62 overexpression NCM460 was constructed (Fig. 6D). NCM460 cells with or without P62 overexpression were treated with CHX at indicated times. The results showed that P62 overexpression promoted the degradation of PFKFB3 (Fig. 6E). P62 were characterized by the ubiquitin binding domains allowing them to bridge cargo (20). It was hypothesized that an E3 ubiquitin ligase mediated PFKFB3 ubiquitination which was recognized by P62. Using the UbiBrowser, E3 ubiquitin ligase prediction website, it was

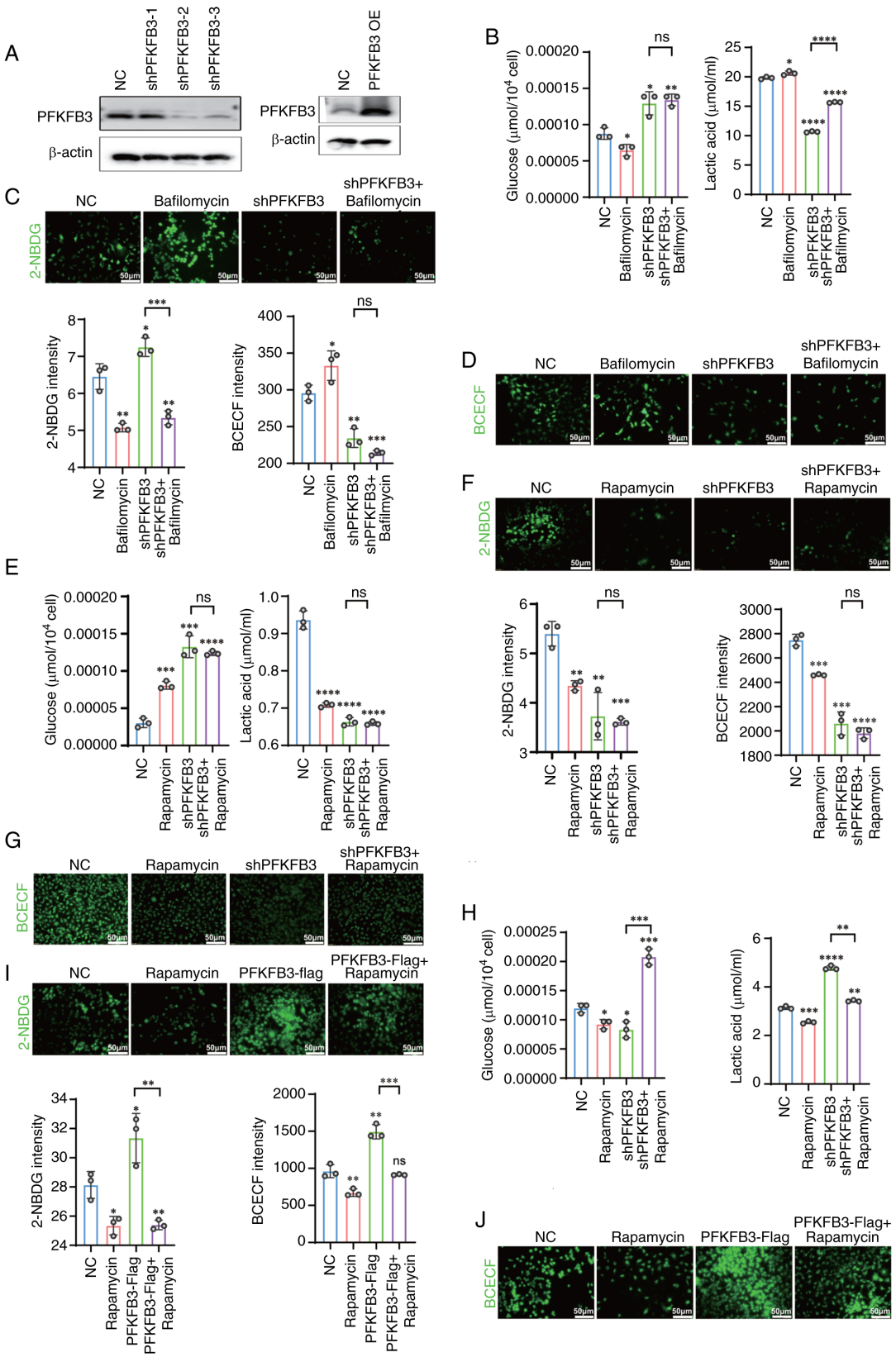

Figure 5. PFKFB3 played a key role in autophagy regulating of the glycolysis of IECs. (A) The verification of PFKFB3 knockdown and overexpression by western blotting. Relative glucose content and Lac production in PFKFB3 knockdown IECs treated with (B) Baf A1 (200 nM) or (E) rapamycin (200 nM). (C and F) 2-NBDG and (D and G) BCECF fluorescent counter-staining in rapamycin or BafA1 treated PFKFB3 knockdown IECs vs. control. Representative immunofluorescence images are shown. (Original magnification, x20) with quantitative fluorescence intensity of 2-NBDG and BCECF (n=3). (H) Relative glucose content and Lac production in PFKFB3 OE IECs treated with rapamycin (200 nM). (I) 2-NBDG and (J) BCECF fluorescent counter-staining in rapamycin treated PFKFB3 OE IECs vs. control. Representative immunofluorescence images are shown (Original magnification, x20) and quantitative fluorescence intensity of 2-NBDG and BCECF (n=3). P-values were calculated using One-way ANOVA followed by Tukey's post-hoc test. The values were presented as the means ± SEM, *P<0.05, **P<0.01, ***P<0.001, ****P<0.0001. PFKFB3, 6-phosphofructo-2-kinase/fructose-2,6-bisphosphatase 3; Lac, lactate; IECs, intestinal epithelial cells; Baf A1, bafilomycin A1; 2-NBDG, 2-deoxy-2-[(7-nitro-2,1,3-benzoxadiazol-4-yl) amino]-D-glucose; BCECF, 2',7'-bis(carboxyethyl)-5(6)-carboxyfluorescein; OE, overexpression.

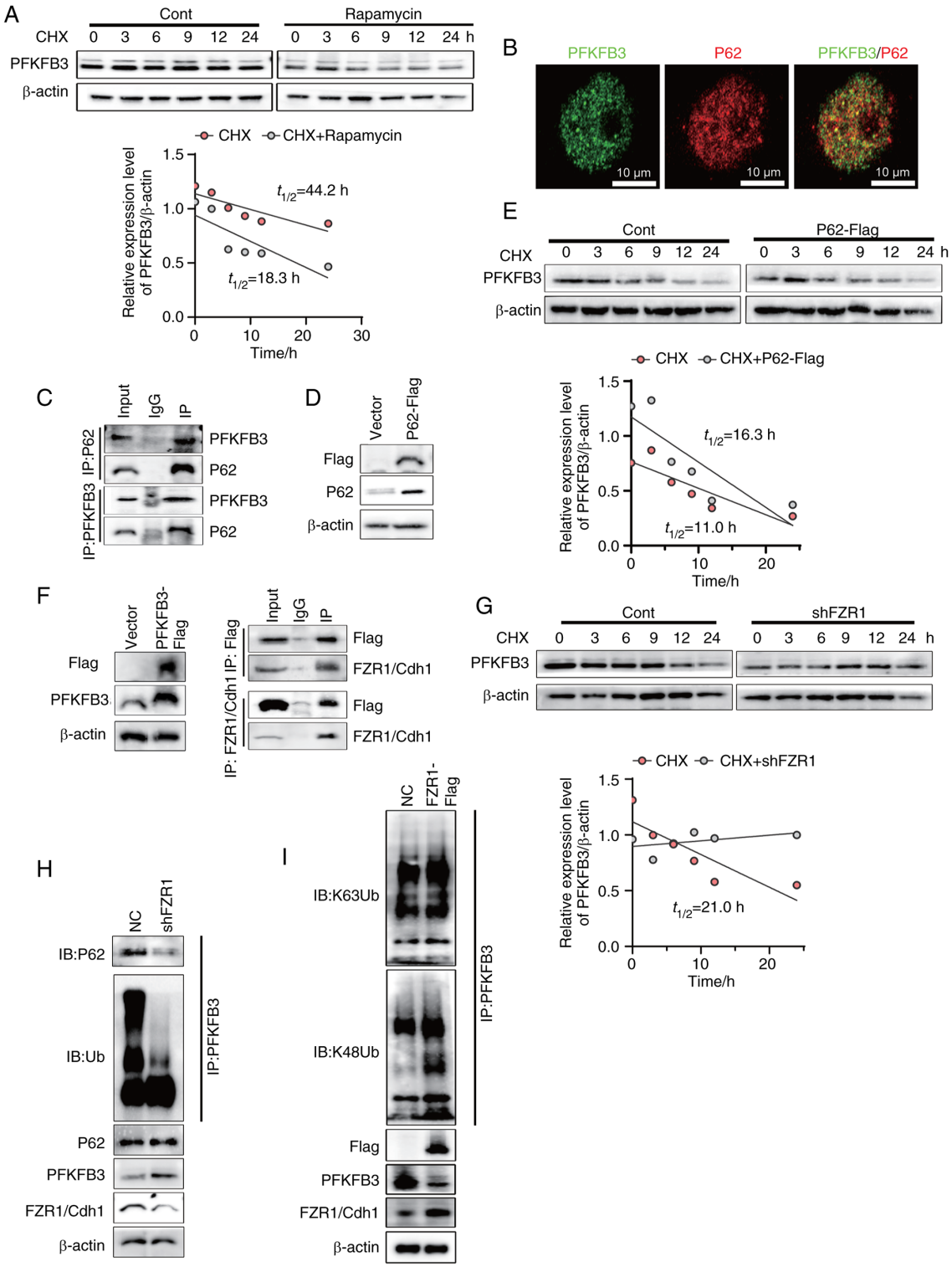

Figure 6. Mechanism of autophagy ubiquitination degrading PFKFB3 protein. (A) NCM460 cells were treated with rapamycin (200 nM) and cells were collected after treatment with 100 μg/ml CHX at the indicated time. The protein levels of PFKFB3 were detected by western blotting. A total of three independent experiments were repeated. (B) Representative images of the NCM460 stained with PFKFB3 and P62. Scale bar, 10 μm. (C) Immunoprecipitation assays of NCM460 cells with anti-PFKFB3 and anti-P62 followed by immunoblotting with antibodies against the indicated proteins. (D) Verification of Flag-tagged P62/SQSTM1 overexpression NCM460 cells by western blotting. (E) Flag-tagged P62/SQSTM1 overexpression NCM460 cells were collected after being treated with 100 μg/ml CHX at the indicated time. The protein levels of PFKFB3 were detected by western blotting. A total of three independent experiments were repeated. (F) Verification of Flag-tagged PFKFB3 overexpression NCM460 cells by western blotting. Immunoprecipitation assays of Flag-tagged PFKFB3 NCM460 cells with anti-Flag and anti-FZR1/Cdh1 followed by immunoblotting with antibodies against the indicated proteins. (G) FZR1 knockdown NCM460 cells were collected after treated with 100 μg/ml CHX at the indicated time. The protein levels of PFKFB3 were detected by western blotting. A total of three independent experiments were repeated. (H) FZR1 knockdown NCM460 cells were transfected with HA-Ub plasmid. Immunoprecipitated PFKFB3 proteins were analyzed by immunoblot analysis for ubiquitination and P62. The protein levels of P62, PFKFB3 and FZR1/Cdh1 were detected in FZR1 knockdown NCM460 cells by western blotting. (I) Cells overexpressing Flag-tagged FZR1 were transfected with the HA-Ub plasmid. Immunoprecipitation of PFKFB3 was performed to assess the levels of K63- and K48-linked polyubiquitin chains via western blotting. Western blot analysis was further used to determine the protein expression levels of Flag, PFKFB3 and FZR1/Cdh1 in FZR1-overexpressing NCM460 cells. PFKFB3, 6-phosphofructo-2-kinase/fructose-2,6-bisphosphatase 3; CHX, cycloheximide; HA-Ub, hemagglutinin-tagged ubiquitin; FZR1, Fizzy and cell division cycle 20 related 1.

found that FZR1/Cdh1 might be the E3 ubiquitin ligase of PFKFB3 in intestinal epithelial cells. To verify this hypothesis, Flag-tagged PFKFB3 overexpression cells were constructed and the interaction of PFKFB3 with FZR1/Cdh1 was analyzed by coimmunoprecipitation (Fig. 6F). Subsequently, to verify the effect of E3 ubiquitin ligase FZR1/Cdh1 on the degradation of PFKFB3, FZR1 knockdown NCM460 cells were constructed. With or without FZR1 knockdown, NCM460 cells were treated with CHX at the indicated times. FZR1 knockdown NCM460 cells and control group were treated with CHX. The remaining PFKFB3 proteins were detected and FZR1 knockdown inhibited the degradation of PFKFB3 (Fig. 6G). Finally, endogenous PFKFB3 ubiquitination levels were analyzed in FZR1 knockdown cells. FZR1 knockdown led to the decreased incorporation of ubiquitin. Furthermore, FZR1 knockdown disrupted the interaction between P62 and PFKFB3. FZR1 knockdown increased the expression of PFKFB3 while P62 was not affected (Fig. 6H). The E3 ubiquitin ligase catalyzed the formation of eight potential isomeric ubiquitin chains by conjugating ubiquitin to one of the seven lysine residues or the N-terminal methionine of the substrate. As specific molecular tags, these ubiquitin chains directed the substrate toward distinct biological outcomes, a concept referred to as the ubiquitin code. Of these, K48- and K63-linked polyubiquitin chains are the two most prevalent types (21). The E3 ubiquitin ligase exhibits inherent selectivity in ubiquitin chain linkage formation (22). To investigate this specificity, an *in vitro* analysis of the ubiquitin chains generated by FZR1 was performed, focusing on K48- and K63-linked polyubiquitin chains. The results demonstrated that FZR1 predominantly promoted the assembly of K48-linked ubiquitin chains, with minimal effect on the formation of K63-linked chains (Fig. 6I). These results indicated that FZR1/Cdh1 mediated the formation of K48-linked ubiquitin chains on PFKFB3, which were subsequently recognized by p62 and delivered via autophagosomes to lysosomes in intestinal epithelial cells for degradation.

Elevated PFKFB3 protein is observed in the colonic epithelium of IBD. To clarify the key role of PFKFB3 in IBD, the expression of PFKFB3 was investigated in IBD. The present study evaluated PFKFB3 expression using RNA sequencing (RNA-seq) datasets from Gene Expression Omnibus (GEO). Results indicated that PFKFB3 was upregulated in CD group, compared with normal tissues group (Fig. 7A). PFKFB3 mRNA levels were further detected in the blood and tissues of patients with CD. The mRNA expression of PFKFB3 in the blood of patients with CD in both active and remission stages were markedly higher than of normal patients. In addition, the elevated mRNA expression of PFKFB3 was also observed in the tissues of patients with CD (Fig. 7B). The expression of PFKFB3 is displayed by immunohistochemical staining of intestinal epithelium of patients with CD (Fig. 7C). To further validate, PFKFB3 and E-cadherin fluorescence staining in colon tissue of patients with CD were performed (Fig. 7D). E-cadherin was one of the epithelial marker proteins. The expression of PFKFB3 in intestinal epithelium was elucidated by co-localization of PFKFB3 with E-cadherin. Semiquantitative analysis of immunohistochemical staining and fluorescence intensity revealed that PFKFB3 highly expression in patients with CD' colonic epithelium tissue.

The expression of PFKFB3 was further observed in colitis mouse model. First, colonic epithelial cells were extracted from mouse model of DSS induced colitis and the PFKFB3 protein level detected in IECs by western blotting. It showed that the expression of PFKFB3 protein was elevated both in acute and chronic colitis model (Fig. 7E). PFKFB3 and E-cadherin immunofluorescence staining were performed. The result of fluorescence co-localization of PFKFB3 and E-cadherin in colitis mouse model revealed that PFKFB3 expression was elevated in colitis colonic epithelium (Fig. 7F). The above results suggested that PFKFB3 plays an important role in inflammatory bowel disease.

PFKFB3 regulates tight junction proteins and inflammatory factors in the intestinal epithelium. Given that the findings proved that the expression of PFKFB3 increased in IBD. To verify whether PFKFB3 as a therapeutic target could alleviate colitis in mice, the present study established DSS-induced colitis mice and treated them with PFK15, a PFKFB3 inhibitor. The colonic morphology of four groups was observed by hematoxylin and eosin staining. Compared with the normal group, the colon villi of mice in DSS colitis group were destroyed and a large number of neutrophils were infiltrated. However, the villus morphology of DSS-induced colitis mice markedly recovered after treatment with PFK15 (Fig. 7G). Immunohistochemical staining assays of claudin-5, claudin-8, claudin-2 and occludin were performed in colons of four groups mice. Among them, claudin-5, claudin-8 and occludin increased interepithelial resistance and decreased barrier permeability, while claudin-2 was found to increase paracellular barrier permeability. The results showed that the expression of claudin-5, claudin-8 and occludin decreased in DSS group, while the expression of claudin-2 increased. Following PFK15 treatment, claudin-5, claudin-8, occludin and claudin-2 recovered (Fig. 7H). mRNA levels of intestinal epithelial cells in four groups of mice were examined and it was found that the inflammatory cytokines, including IL-6, TNF-α and IL-1β, decreased markedly after PFK15 treatment (Fig. 7I).

Discussion

Autophagy is involved in intestinal homeostasis and repair by mediating the recycling of organelles and protein aggregates, as well as the destruction of intracellular pathogens (23). Impaired intestinal autophagy results in the disruption of intestinal epithelial barrier, increased intestinal permeability, impaired antimicrobial peptide secretion, promotion of apoptosis of intestinal epithelial cells and excessive accumulation of ROS (24). Impaired autophagy is observed in mouse colitis models, LPS-induced IEC inflammation models and IECs inpatients with active CD (4,25,26). The present study also found impaired autophagy both in colonic epithelial cells of DSS induced colitis mice and TNF-α induced NCM460 cells.

Glycolysis is a metabolic process of glucose in the cytoplasm to produce energy and metabolites for macromolecular biosynthesis. Glycolysis involved the conversion of glucose to pyruvate and the conversion of pyruvate to lactic acid (27). The mRNA levels of key glycolysis enzymes are elevated in the blood of patients with IBD (12). Moreover, lactic acid

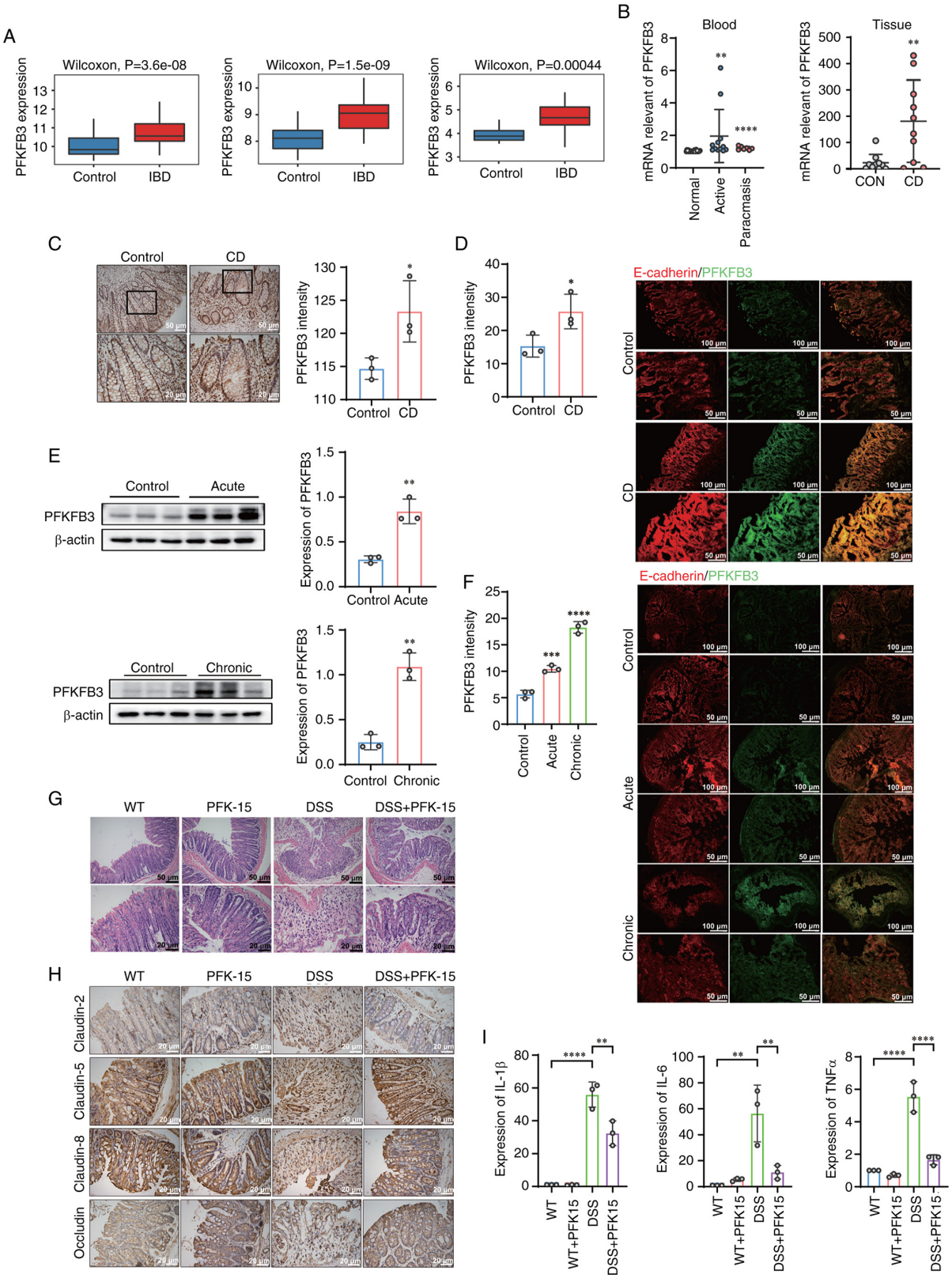

Figure 7. PFKFB3 was upregulated in IBD. (A) Analysis of PFKFB3 mRNA expression in normal and Crohn's disease tissues within public datasets (GSE119600, GSE126124, GSE112057). (B) mRNA levels of PFKPFB3 in control (n=10) vs. tissue of patients with Crohn's disease (n=10), control (n=26) vs. blood of patients with Crohn's disease (active stage n=12; remission stage n=7). (C) Immunohistochemical staining of PFKFB3 in tissue of patients with Crohn's disease and semiquantitative analysis (n=3). (D) Immunofluorescence images of PFKFB3 in colonic epithelial tissue of patients with Crohn's disease and quantification of the fluorescence intensity of PFKFB3 (n=3). (E) Protein levels of PFKFB3 in control vs. colonic epithelium of DSS-induced mice (acute n=3, chronic n=3). (F) Immunofluorescence images of PFKFB3 in colonic epithelium of DSS-induced mice and quantification of the fluorescence intensity of PFKFB3 (acute n=3, chronic n=3). (G) Representative hematoxylin and eosin staining of the colon. DSS-induced colitis mice were treated with intraperitoneal injection of PFK-15 every three days. (H) Immunohistochemical staining of claudin-5, claudin-8, claudin-2 and occludin in colon tissue. (I) mRNA levels of IL-6, TNF-α and IL-1β. The P values for all figures except B, F, and H were calculated using unpaired t-tests, while one-way ANOVA followed by Tukey's multiple comparisons test was used for B, F and H. The values were presented as the means ± SEM, *P<0.05, **P<0.01, ***P<0.001, ****P<0.0001. PFKFB3, 6-phosphofructo-2-kinase/fructose-2,6-bisphosphatase 3; IBD, inflammatory bowel disease; DSS, dextran sulfate sodium salt; PFK-1, phosphofructokinase-1; CD, Crohn's disease; WT, Wild-type.

production is increased in mice with IL-10-deficient idiopathic colitis (28). Khaloian *et al* (15) also indicated that inhibition of glycolysis was able to alleviate intestinal stem cells damage caused by inflammation. Consistent with these, the present study also found increased glycolysis level in the inflammatory NCM460 cells. Furthermore, mRNA levels of key glycolytic enzymes PFKFB3, LDHA and PFKP were elevated in colon IECs from DSS-induced colitis.

Increasing evidence suggests a mutually regulatory relationship between autophagy and glycolysis (29). For example, inhibition of PKM2 enzymatic activity activates autophagy in lung carcinoma cell lines (30). Sorafenib-induced autophagy promotes glycolysis by elevated glycolytic enzyme PKM2 activity in hepatocellular carcinoma cells (31). The present study found that autophagy negatively regulated glycolysis by the degradation of PFKFB3 in IECs. Therefore, the findings suggested a significant correlation between autophagy in the intestinal epithelium and metabolic processes.

PFKFB3 protein is one of the isoenzymes of PFK-2/FBPase-2 and is mainly responsible for the conversion of fructose-6-phosphat to fructose-2,6-bisphosphate. With the highest kinase/phosphatase ratio among all PFK/FBPase-2 family members, PFKFB3 promotes increased cellular glycolysis flux (32). The present study also demonstrated that lactic acid production increased in an PFKFB3-dependent manner *in vitro*.

To further elucidate the mechanism of PFKFB3 autophagic degradation, the present study first identified the autophagy receptor for PFKFB3. Multiple autophagy receptors, such as NDP52, OPTN, p62, and TAX1BP1, are capable of specifically recognizing cargo proteins (20). PFKFB3 is reported as an autophagy substrate bound to P62 in breast cancer stem cells (33). Consistently, the results of our preliminary immunoprecipitation experiment also demonstrated P62 interacted with PFKFB3. For P62, it interacted with ubiquitinated cargo due to its C-terminal UBA domain (19). Based on this, the present study predicted and screened FZR1/Cdh1 as a PFKFB3 ubiquitination E3 ligase using the UbiBrowser website. PFKFB3 is degraded by ubiquitination of FZR1/Cdh1 in astrocytes from rat brains (34). Notably, the present study also found that FZR1/Cdh1 interacted with PFKFB3 in NCM460 cells and the degradation of PFKFB3 was mediated by FZR1/Cdh1 ubiquitination. Mechanistic analysis revealed that the K48-linked polyubiquitin chain served as the specific ubiquitin code mediating FZR1/Cdh1-induced degradation of PFKFB3 in intestinal epithelial cells.

Subsequently, the present study investigated the important effect of PFKFB3 on IBD. Inhibition of PFKFB3 activity reduced inflammatory damage in DSS-induced colitis. Zhou *et al* (35) also reported increased stromal PFKFB3-mediated glycolysis contributed to intestinal inflammation in IBD. In addition, inhibited PFKFB3 activity with PFK-15 prevented DSS induced reduction of claudin-5, claudin-8 and occludin and increase of claudin-2 in colonic epithelium. Claudin-5, claudin-8 and occludin are known as 'Sealing' tight junction proteins maintaining intestinal barrier integrity. By contrast, the leaking protein claudin-2 is reported to increase barrier permeability (36). The above results revealed that inhibition of PFKFB3 expression could reduce inflammatory damage in IBD and restored intestinal barrier function. In addition, the present study underscored the critical interplay between intestinal metabolism and inflammation, offering novel insights into the regulation of intestinal epithelial metabolism in IBD and suggesting potential avenues for therapeutic development.

A previous study demonstrated that urinary lactate levels accurately reflect PFKFB3-mediated glycolytic abnormalities and declining renal function in patients with chronic kidney disease (CKD), suggesting their potential as a biomarker for monitoring CKD progression (37). These findings raise an important question: Could fecal lactate levels similarly reflect PFKFB3-driven glycolytic dysregulation in IECs and serve as a non-invasive biomarker for identifying IBD? At this stage, it was recognized that the present study still had certain limitations.

The present study demonstrated through both *in vivo* and *in vitro* experiments that PFKFB3 intervention exerted a significant therapeutic effect on intestinal damage associated with IBD. Currently, the PFKFB3 small molecule inhibitor has entered Phase I clinical trials and preliminary results have demonstrated its favorable safety profile and promising anti-cancer activity in patients with cancer (38). Accumulating evidence indicates that PFKFB3 is closely linked to intestinal inflammatory responses, suggesting the potential therapeutic utility of this inhibitor in the clinical management of IBD. To facilitate the clinical translation of PFKFB3 inhibitors, future research should prioritize the development of advanced delivery systems, such as nanocarriers or targeted encapsulation platforms, to minimize systemic toxicity and improve tissue-specific targeting. Such an approach could markedly accelerate the clinical application of PFKFB3-targeted therapies for IBD treatment.

Based on the findings of the present study, a novel strategy for combined autophagy and glycolysis-targeted therapy in the treatment of IBD is proposed. Currently used clinical therapeutics for IBD, such as corticosteroids and 5-aminosalicylic acid, may exert part of their therapeutic effects through inhibition of the glycolytic pathway (39). Meanwhile, a growing number of studies have focused on developing therapeutic strategies for IBD by modulating autophagy, with some promising advances achieved (40-42). However, autophagy-based therapies primarily aim to maintain the dynamic equilibrium of autophagic activity in intestinal cells, rather than merely activating or inhibiting the process. Consequently, precise control of drug dosage remains a significant challenge (43). Although the dual-targeted combined therapy strategy that simultaneously modulates autophagy and glycolysis holds therapeutic potential, it may also give rise to drug efficacy interference due to pharmacological interactions. Moreover, the systemic physiological consequences of multi-pathway interventions require thorough assessment. Therefore, precise optimization of dosage regimens and temporal administration schedules will be critical in determining the clinical viability of this approach. It is noteworthy that recent studies have demonstrated that specific dietary components can alleviate intestinal symptoms of IBD by modulating intestinal autophagy (44). These findings suggest that combining pharmacological inhibition of abnormal intestinal glycolysis with dietary interventions targeting autophagy regulation may enhance the therapeutic efficacy of IBD treatment.

In conclusion, increase of PFKFB3-mediated glycolysis in IECs is involved in IBD intestinal inflammatory damage and epithelial barrier breakdown. Autophagy in IECs could inhibit glycolysis and maintain intestinal homeostasis by selective degradation of PFKFB3. The present study indicated that PFKFB3 was both a key glycolytic enzyme and an autophagy substrate, establishing crosstalk between autophagy and glycolysis in IECs. Combined therapy targeting autophagy and glycolysis might become a new choice for clinical treatment of IBD.

Acknowledgements

Not applicable.

Funding

The present study was supported in part by grants from Natural Science Foundation of Chongqing (grant no. CSTB2023NSCQ-MSX0027 to Min Yu), grants from the National Natural Science Foundation of China (grant no. NSFC 81970468 to Min Yu), grants from the National Natural Science Foundation of China (grant no. NSFC 82270585 to Weidong Xiao) and grants from the Senior Medical Talents Program of Chongqing for Young and Middle-aged (Min Yu).

Availability of data and materials

The data generated in the present study may be requested from the corresponding author.

Authors' contributions

The project was designed and directed by MY, WX, TY and HY. The experiments were performed by YP and FY. MY, YP and FY analyzed the data. MY and YP wrote the manuscript. GD, LW and CX collected clinical samples. MY, FY and YP confirm the authenticity of all the raw data. All authors read and approved the final manuscript.

Ethics approval and consent to participate

All animal procedures were performed under the guidelines of the Laboratory Animal Welfare and Ethics Committee of the Third Military Medical University (approval no. AMUWEC20224496) and was approved by the Laboratory Animal Welfare and Ethics Committee of the Third Military Medical University (approval no. AMUWEC20224496). Patient tissue collection followed the guidelines and principles of the Helsinki Declaration and received approval from the Ethics Committee of Second Affiliated Hospital of Army Medical University (approval no. 2022-188-01). Written informed consent was obtained from all study participants.

Patient consent for publication

Not applicable.

Competing interests

The authors declare that they have no competing interests.

References

1. Li S, Zhang F and Zhang Q: Pathological features-based targeted delivery strategies in IBD therapy: A mini review. Biomed Pharmacother 151: 113079, 2022.
2. Torres J, Mehandru S, Colombel JF and Peyrin-Biroulet L: Crohn's disease. Lancet 389: 1741-1755, 2017.
3. Mizushima N and Komatsu M: Autophagy: Renovation of cells and tissues. Cell 147: 728-741, 2011.
4. Foerster EG, Mukherjee T, Cabral-Fernandes L, Rocha JDB, Girardin SE and Philpott DJ: How autophagy controls the intestinal epithelial barrier. Autophagy 18: 86-103, 2022.
5. Saha K, Ganapathy AS, Wang A, Morris NM, Suchanec E, Ding W, Yochum G, Koltun W, Nighot M, Ma T and Nighot P: Autophagy reduces the degradation and promotes membrane localization of occludin to enhance the intestinal epithelial tight junction barrier against paracellular macromolecule flux. J Crohns Colitis 17: 433-449, 2023.
6. Aden K, Tran F, Ito G, Sheibani-Tezerji R, Lipinski S, Kuiper JW, Tschurtschenthaler M, Saveljeva S, Bhattacharyya J, Häsler R, *et al*: ATG16L1 orchestrates interleukin-22 signaling in the intestinal epithelium via cGAS-STING. J Exp Med 215: 2868-2886, 2018.
7. Zhou C, Li L, Li T, Sun L, Yin J, Guan H, Wang L, Zhu H, Xu P, Fan X, *et al*: SCFAs induce autophagy in intestinal epithelial cells and relieve colitis by stabilizing HIF-1alpha. J Mol Med (Berl) 98: 1189-1202, 2020.
8. Pral LP, Fachi JL, Corrêa RO, Colonna M and Vinolo MAR: Hypoxia and HIF-1 as key regulators of gut microbiota and host interactions. Trends Immunol 42: 604-621, 2021.
9. Rath E, Moschetta A and Haller D: Mitochondrial function-gatekeeper of intestinal epithelial cell homeostasis. Nat Rev Gastroenterol Hepatol 15: 497-516, 2018.
10. Ho GT and Theiss AL: Mitochondria and inflammatory bowel diseases: Toward a stratified therapeutic intervention. Ann Rev Physiol 84: 435-459, 2022.
11. Adolph TE, Meyer M, Schwärzler J, Mayr L, Grabherr F and Tilg H: The metabolic nature of inflammatory bowel diseases. Nat Rev Gastroenterol Hepatol 19: 753-767, 2022.
12. Vermeulen N, Vermeire S, Arijs I, Michiels G, Ballet V, Derua R, Waelkens E, Van Lommel L, Schuit F, Rutgeerts P and Bossuyt X: Seroreactivity against glycolytic enzymes in inflammatory bowel disease. Inflamm Bowel Dis 17: 557-564, 2011.
13. Shimshoni E, Ghini V, Solomonov I, Luchinat C, Sagi I and Turano P: Integrated metabolomics and proteomics of symptomatic and early pre-symptomatic states of colitis. bioRxiv: doi: https://doi.org/10.1101/2020.03.22.002196.
14. Hamade H, Stamps JT, Stamps DT, More SK, Thomas LS, Blackwood AY, Lahcene NL, Castanon SL, Salumbides BC, Shimodaira Y, *et al*: BATF3 protects against metabolic syndrome and maintains intestinal epithelial homeostasis. Front Immunol 13: 841065, 2022.
15. Khaloian S, Rath E, Hammoudi N, Gleisinger E, Blutke A, Giesbertz P, Berger E, Metwaly A, Waldschmitt N, Allez M and Haller D: Mitochondrial impairment drives intestinal stem cell transition into dysfunctional Paneth cells predicting Crohn's disease recurrence. Gut 69: 1939-1951, 2020.
16. Livak KJ and Schmittgen TD: Analysis of relative gene expression data using real-time quantitative PCR and the 2 (-Delta Delta C(T)) method. Methods 25: 402-408, 2001.
17. Levine B and Kroemer G: Biological functions of autophagy genes: A disease perspective. Cell 176: 11-42, 2019.
18. Collier JJ, Oláhová M, McWilliams TG and Taylor RW: ATG7 safeguards human neural integrity. Autophagy 17: 2651-2653, 2021.
19. Lane JD, Korolchuk VI, Murray JT, Lamark T, Svenning S and Johansen T: Regulation of selective autophagy: The p62/SQSTM1 paradigm. Essays in Biochemistry 61: 609-624, 2017.
20. Vargas JNS, Hamasaki M, Kawabata T, Youle RJ and Yoshimori T: The mechanisms and roles of selective autophagy in mammals. Nat Rev Mol Cell Biol 24: 167-185, 2022.
21. Ohtake F, Saeki Y, Ishido S, Kanno J and Tanaka K: The K48-K63 branched ubiquitin chain regulates NF-κB signaling. Mol Cell 64: 251-266, 2016.
22. Renz C, Asimaki E, Meister C, Albanèse V, Petriukov K, Krapoth NC, Wegmann S, Wollscheid HP, Wong RP, Fulzele A, *et al*: Ubiquiton-An inducible, linkage-specific polyubiquitylation tool. Mol Cell 84: 386-400.e311, 2024.
23. Telpaz S and Bel S: Autophagy in intestinal epithelial cells prevents gut inflammation. Trends Cell Biol 33: 817-819, 2023.

24. Larabi A, Barnich N and Nguyen HTT: New insights into the interplay between autophagy, gut microbiota and inflammatory responses in IBD. Autophagy 16: 38-51, 2020.
25. Zhou M, Xu W, Wang J, Yan J, Shi Y, Zhang C, Ge W, Wu J, Du P and Chen Y: Boosting mTOR-dependent autophagy via upstream TLR4-MyD88-MAPK signalling and downstream NF-kappaB pathway quenches intestinal inflammation and oxidative stress injury. EBioMedicine 35: 345-360, 2018.
26. Shi W, Peng K, Yu H, Wang Z, Xia S, Xiao S, Tian D, Vallance BA and Yu Q: Autotaxin (ATX) inhibits autophagy leading to exaggerated disruption of intestinal epithelial barrier in colitis. Biochim Biophys Acta Mol Basis Dis 1869: 166647, 2023.
27. Bian X, Jiang H, Meng Y, Li YP, Fang J and Lu Z: Regulation of gene expression by glycolytic and gluconeogenic enzymes. Trends Cell Biol 32: 786-799, 2022.
28. Martin FP, Rezzi S, Philippe D, Tornier L, Messlik A, Hölzlwimmer G, Baur P, Quintanilla-Fend L, Loh G, Blaut M, *et al*: Metabolic assessment of gradual development of moderate experimental colitis in IL-10 deficient mice. J Proteome Res 8: 2376-2387, 2009.
29. Yang J, Zhou RM and Ma ZY: Autophagy and energy metabolism. Autophagy: Biology and diseases: Basic Science 1206: 329-357, 2019.
30. Prakasam G, Singh RK, Iqbal MA, Saini SK, Tiku AB and Bamezai RNK: Pyruvate kinase M knockdown-induced signaling via AMP-activated protein kinase promotes mitochondrial biogenesis, autophagy, and cancer cell survival. J Biol Chem 292: 15561-15576, 2017.
31. Yan X, Tian R, Sun J, Zhao Y, Liu B, Su J, Li M, Sun W and Xu X: Sorafenib-induced autophagy promotes glycolysis by upregulating the p62/HDAC6/HSP90 axis in hepatocellular carcinoma cells. Front Pharmacol 12: 788667, 2022.
32. Kotowski K, Rosik J, Machaj F, Supplitt S, Wiczew D, Jabłońska K, Wiechec E, Ghavami S and Dzięgiel P: Role of PFKFB3 and PFKFB4 in cancer: Genetic basis, impact on disease development/progression, and potential as therapeutic targets. Cancers (Basel) 13: 909, 2021.
33. La Belle Flynn A, Calhoun BC, Sharma A, Chang JC, Almasan A and Schiemann WP: Autophagy inhibition elicits emergence from metastatic dormancy by inducing and stabilizing Pfkfb3 expression. Nat Commun 10: 3668, 2019.
34. Almeida A, Bolaños JP and Moncada S: E3 ubiquitin ligase APC/C-Cdh1 accounts for the Warburg effect by linking glycolysis to cell proliferation. Proc Natl Acad Sci USA 107: 738-741, 2009.
35. Zhou Z, Plug LG, Patente TA, de Jonge-Muller ESM, Elmagd AA, van der Meulen-de Jong AE, Everts B, Barnhoorn MC and Hawinkels LJAC: Increased stromal PFKFB3-mediated glycolysis in inflammatory bowel disease contributes to intestinal inflammation. Front Immunol 13: 2022.
36. Pan YY, Deng Y, Su S, Yin JH, Chen YH, Wang LC, Sun LH, Xiao WD and Du GS: Structure composition and intracellular transport of clathrin-mediated intestinal transmembrane tight junction protein. Inflammation 46: 18-34, 2022.
37. Wang Y, Li H, Jiang S, Fu D, Lu X, Lu M, Li Y, Luo D, Wu K, Xu Y, *et al*: The glycolytic enzyme PFKFB3 drives kidney fibrosis through promoting histone lactylation-mediated NF-κB family activation. Kidney Int 106: 226-240, 2024.
38. Shi L, Pan H, Liu Z, Xie J and Han W: Roles of PFKFB3 in cancer. Signal Transduct Target Ther 2: 17044, 2017.
39. Chen N, Xie QM, Song SM, Guo SN, Fang Y, Fei GH and Wu HM: Dexamethasone protects against asthma via regulating Hif-1α-glycolysis-lactate axis and protein lactylation. Int Immunopharmacol 131: 111791, 2024.
40. Zhang H, Cui Z, Cheng D, Du Y, Guo X, Gao R, Chen J, Sun W, He R, Ma X, *et al*: RNF186 regulates EFNB1 (ephrin B1)-EPHB2-induced autophagy in the colonic epithelial cells for the maintenance of intestinal homeostasis. Autophagy 17: 3030-3047, 2021.
41. Yuan S, Liu BH, Cheng WW, Meng H, Hou XT, Xue JC, Zhang HM and Zhang QG: Polyphyllin VI modulates macrophage polarization through autophagy-NLRP3 inflammasome to alleviate inflammatory bowel disease. Phytomedicine 143: 156640, 2025.
42. Retnakumar SV and Muller S: Pharmacological autophagy regulators as therapeutic agents for inflammatory bowel diseases. Trends Mol Med 25: 516-537, 2019.
43. Shao BZ, Yao Y, Zhai JS, Zhu JH, Li JP and Wu K: The role of autophagy in inflammatory bowel disease. Front Physiol 12: 621132, 2021.
44. Zhou M, Zhi J, Zhi J, Xiong Z, Wu F, Lu Y and Hu Q: Polysaccharide from Strongylocentrotus nudus eggs regulates intestinal epithelial autophagy through CD36/PI3K-Akt pathway to ameliorate inflammatory bowel disease. Int J Biol Macromol 244: 125373, 2023.